

RESEARCH ARTICLE

10.1002/2015JA021714

Key Points:

- E_y ranged from 0.19 to 0.35 mV/m between 8 and 18 h (LT) in the Brazilian sector
- E_z ranged from 4.65 to 10.12 mV/m between 8 and 18 h (LT) in the Brazilian sector
- E_z show a more pronounced dependence of the solar activity, based on the $F_{10.7}$

Correspondence to:

C. M. Denardini,
clezio.denardin@inpe.br

Citation:

Denardini, C. M., J. Moro, L. C. A. Resende, S. S. Chen, N. J. Schuch, and J. E. R. Costa (2015), *E* region electric field dependence of the solar activity, *J. Geophys. Res. Space Physics*, 120, 8934–8941, doi:10.1002/2015JA021714.

Received 21 JUL 2015

Accepted 19 SEP 2015

Accepted article online 23 SEP 2015

Published online 15 OCT 2015

E region electric field dependence of the solar activityC. M. Denardini¹, J. Moro¹, L. C. A. Resende¹, S. S. Chen^{1,2}, N. J. Schuch³, and J. E. R. Costa¹

¹National Institute for Space Research, São José dos Campos, Brazil, ²Department of Electrical Engineering, University of Taubaté, Taubaté, Brazil, ³Southern Regional Space Research Center, INPE, Santa Maria, Brazil

Abstract We have been studying the zonal and vertical *E* region electric field components inferred from the Doppler shifts of type 2 echoes (gradient drift irregularities) detected with the 50 MHz backscatter coherent radar set at São Luis, Brazil (SLZ, 2.3°S, 44.2°W) during the solar cycle 24. In this report we present the dependence of the vertical and zonal components of this electric field with the solar activity, based on the solar flux $F_{10.7}$. For this study we consider the geomagnetically quiet days only ($Kp \leq 3^+$). A magnetic field-aligned-integrated conductivity model was developed for proving the conductivities, using the IRI-2007, the MISIS-2000, and the IGRF-11 models as input parameters for ionosphere, neutral atmosphere, and Earth magnetic field, respectively. The ion-neutron collision frequencies of all the species are combined through the momentum transfer collision frequency equation. The mean zonal component of the electric field, which normally ranged from 0.19 to 0.35 mV/m between the 8 and 18 h (LT) in the Brazilian sector, show a small dependency with the solar activity. Whereas the mean vertical component of the electric field, which normally ranges from 4.65 to 10.12 mV/m, highlights the more pronounced dependency of the solar flux.

1. Introduction

The equatorial electrojet (EEJ) is an intense electric current flowing at about 105 km of altitude in the equatorial *E* region and covering a latitudinal range of $\pm 5^\circ$ around the dip equator. It is basically driven by the *E* region dynamo electric field [Fejer and Kelley, 1980] and represents an important aspect of the phenomenology of the equatorial ionosphere-thermosphere system. Magnetic observations of the ground-derived EEJ strength have been studied in several longitudinal sectors for many years [Sugiura and Cain, 1966; Mayaud, 1977; Campbell, 1989, and references therein]. Sounding observations of the equatorial ionospheric *E* region using VHF radars have been reported since the 1960s. Apart from some radar sounding campaigns, most of the backscattered echoes from electron density irregularities in the EEJ have been routinely acquired only in the Peruvian sector [Farley, 1963; Cohen and Bowles, 1967; Cohen, 1973; Farley, 1985; Hysell and Burcham, 2000] and the Indian sector [Prakash *et al.*, 1971; Reddy and Devasia, 1976, 1981; Patra *et al.*, 2005].

Since the 2000s, several aspects of the EEJ were also investigated based on the coherent radar technique in the Brazilian sector: the vertical distributions of the irregularities type 1 and type 2 [Denardini *et al.*, 2003], the day-to-day variabilities of the EEJ under auroral activity and quiet conditions [Denardini *et al.*, 2004], its seasonal characterization [Denardini *et al.*, 2005], and the transition from daytime to nighttime [Denardini *et al.*, 2006], when the prereversal electrodynamic enhancement lifts the whole ionosphere leading to formation of the plasma bubbles. Also, specifically about the responses of the *E* regions electric field (EF), drivers of the EEJ, to storm time, significant progress have been made by Denardini *et al.* [2009, 2011] to explain the behavior of the plasma irregularities (driven by electric field) to the disturbance dynamo. In addition, Shume *et al.* [2010, 2011] and Guizzelli *et al.* [2013] investigated the regional differences about the EEJ in the Brazilian and Peruvian sector.

Significant contribution to the understanding of the atmosphere-ionosphere coupling processes at the *E* region height due to upward propagating waves from tropospheric sources was performed by Aveiro *et al.* [2009a, 2009b], when studying the climatology of gravity waves (GW) and the signatures of 2 day wave in the EF. They showed the relationship between the 2 day wave and winds and ionospheric currents, as well as that up to 20% of the EEJ driving electric field can be due to GW-induced electric fields in the equatorial *E* region. Recently, Denardini *et al.* [2013] investigated the anomalous conductivity effects on the EEJ electric fields and its possible dependence of the GW braking at the *E* region heights.

With respect to the solar dependence of the *E* region, it is well known that the EUV, UV, Lyman- α , and X-ray photoionization processes control the electron density along with the whole set of chemical reactions.

Also, Resende and Denardini [2012] and Resende et al. [2013] investigated the evolution of the electron density during solar events of the solar cycle 23 and demonstrated that the E region can be directly affected by the X-ray flow due to solar flare.

In addition to these series of work investigating the physical dependence of the EEJ electric field to several controlling factors in the Brazilian sector, we present the dependence of the vertical and zonal components of this electric field with the solar activity based on the solar flux $F_{10.7}$ in the present paper.

2. Methodology

For the present study, we have selected the coherent VHF backscatter radar data collected during the geomagnetically quiet days ($Kp \leq 3^+$) only, covering the years from 2001 to 2009, collected in the Brazilian dip equator. Based on these radar data we estimate the vertical component of the electric field (E_z), and thereafter, with the aid of a magnetic field-aligned-integrated conductivity model, we derived the zonal component of the electric field (E_y). The diurnal variations of these quantities were then evaluated considering the solar activity during the last solar cycle.

As an indicator of the solar activity, we have used the $F_{10.7}$ solar flux which corresponds to the electromagnetic solar emission at wavelength of 10.7 cm (equivalent to the 2.8 GHz frequency, measured in solar flux unit (sfu), $1 \text{ sfu} = 10^{-22} \text{ W m}^{-2} \text{ Hz}^{-1}$). The integrated solar flux density at 10.7 cm wavelength was used as a proxy for the solar activity due to its known relation to ionizing radiation and terrestrial effects [Chatterjee and Das, 1995]. Therefore, it is commonly used in several ionospheric models. During the present study (2001–2009), the daily averaged $F_{10.7}$ varied from high solar activity (greater than 150 sfu) to low solar activity (below 100 sfu). In the period of high solar activity (2001–2002), the $F_{10.7}$ solar flux was greater than 150 sfu during most of the radar soundings, sometimes peaking 250 sfu. In 2003, there was a decrease in the $F_{10.7}$ flux to values between 100 and 150 sfu. Afterward, the $F_{10.7}$ flux decreased below 100 sfu from 2006 to 2009.

In the following subsection we provide relevant additional information concerning the analysis of solar activity dependence of the diurnal variations of the EF, which includes (a) a basic radar characteristic impacting the data description (e.g., range height and time resolution), (b) the electric field computing from the radar data, and (c) a discussion about the models affecting the electric field computation.

2.1. Basic RESCO Description

The 50 MHz coherent backscatter radar (RESCO) is located at São Luís (2.3°S, 44.2°W), which was an equatorial station up to 2012, before the secular variations of the Earth magnetic field drift the magnetic equator away.

General features are the following: (1) modular system consisting of eight power transmitter phased locked; (2) attainable total power of 120 kW (8×15 kW); (3) coaxial collinear broadside antenna array for transmission and reception consisting of 32 antennas, each antenna having 24 dipoles aligned in the magnetic north-south direction; and (4) two-way oblique beam tilted by 30° in zenith angle, settable in the east-west plane, $\sim 7^\circ$ beam width in both cases and $\sim 5^\circ$ in the north-south plane.

Operations mode used for the present data set are the following:

1. Transmitting peak power was limited to 40 kW (8×5 kW);
2. Oblique beam was tilted westward;
3. Transmitted (noncoded) pulse width was set to 20 μs ;
4. Interpulse period was set to 1 ms;
5. Echo sampling with a 20 μs wide window (3 km in range, about 2.6 km in height);
6. Sampling height was set to 600 μs after each transmitted pulse, and 16 subsequent samples were taken in order to cover the height range from about 80 to 120 km; and
7. Data rate was set to one power spectrum of 512 points per 12 s.

This experiment ran from 2001 to 2009 and 234 magnetically quiet days ($Kp \leq 3^+$) were selected for the present analysis. The electric field values were calculated at the four different radar range heights around the EEJ center: from 101.3 to 103.9 km, centered at 102.5 km; from 103.9 to 106.5 km, centered at 105.1 km; from 106.5 to 109.1 km, centered at 107.7 km, and from 109.1 to 111.7 km, centered at 110.3 km. These

specific altitudes are derived from the radar general features and operations mode used for the getting the data set.

2.2. The Electric Field Computing From the RESCO Radar Data

A spectral decomposition technique was applied to every single spectrum, assuming that the experimental spectra can be decomposed in many Gaussians as stated by *Cohen* [1973]. In the present study, it involved fitting the sum of two Gaussians to the spectrum, which is described by an “S” distribution in function of the frequency, given by equation (1).

$$S(f) = \frac{P_1}{\sigma_1 \sqrt{2\pi}} \exp \left[-\frac{(f - f_{D1})^2}{2\sigma_1^2} \right] + \frac{P_2}{\sigma_2 \sqrt{2\pi}} \exp \left[-\frac{(f - f_{D2})^2}{2\sigma_2^2} \right] + P_N \quad (1)$$

where P_N , $P_{1,2}$, $\sigma_{1,2}$, and $f_{D(1,2)}$ are, respectively, the noise level power, the spectral power, the spectral power width, and the Doppler frequency, and the subscript indicates the type of the EEJ irregularity being considered: type 1 or type 2. The maximum likelihood estimate (MLE) has been then used for nonlinear fitting of the seven parameters of each power spectrum, $\mathbf{a} = \{P_1, \sigma_1, f_{D1}, P_2, \sigma_2, f_{D2}, P_N\}$ in which the fitting method is based on finding the parameters that maximize the probability function $P(y_1 \dots y_{512} | \mathbf{a})$ of obtaining the data set $\mathbf{y} = \{y_1 \dots y_{512}\}$ [Bard, 1974; Press et al., 1992]. The fitted curves with spectral power density smaller than 5% of the maximum spectral power density for the whole day are discarded to avoid eventual bad fitting related problems, usually less than 4.4% of the fitted, depending to the signal-to-noise ratio (SNR) of the echoes collected in each specific day. Those remaining fitted curves have uncertainty from 0.92 up to 5.06% (2.42% in average) for the Doppler velocity determination of the irregularity type 2, depending on (a) the SNR of the echoes collected in each specific day, (b) the number of incoherent power spectra integration, and (c) the simultaneously detection (or no) of the irregularity type 1 in the radio signal. Thereafter, the Doppler frequencies were converted into the Doppler velocities taking into account the radar operating frequency and the speed of light, based on the phase deviation of the received signal. The Doppler velocities from the irregularities type 2 (V_{D2}) obtained from the selected quiet days were grouped according to the height and time of data acquisition, aiming to obtain mean velocities at a given height and local time. Thus, we have the horizontal component of these mean velocities along the radar beam [Balsley, 1969; Cohen, 1973; Hanuise and Crochet, 1978], which relates with its driving electric field as per equation (2).

$$E_z = \frac{1}{\sin(\theta)} \frac{V_{D2}(1 + \psi_0) \cdot B^2}{H} \quad (2)$$

where $\psi_0 = v_e \cdot v_i / \Omega_e \cdot \Omega_i$ (at zero aspect angle), Ω_{ei} is the gyrofrequency, v_{ei} is the collision frequency, and θ is the zenith angle of the radar beam. The subscript “e” and “i” indicates the electron and ion terms, respectively. After obtaining E_z , we used the conductivity model to calculate the Hall (σ_H) and Pedersen (σ_P) conductivities along the magnetic meridian overhead the RESCO radar site with grid resolution of 1 km in both up-down and magnetic north-south directions. Thereafter, we used the magnetic field model to obtain the field line coordinates, as described in *Denardini* [2007], and the E_y are derived as follows:

$$E_y = \frac{\int_{-\theta}^{+\theta} \sigma_P \mathbf{r} \cdot d\theta}{\int_{-\theta}^{+\theta} \sigma_H \mathbf{r} \cdot d\theta} \cdot E_z \Rightarrow E_y = \frac{\sum_P}{\sum_H} \cdot E_z. \quad (3)$$

2.3. Discussion About the Models Effecting the Electric Field Computation

In order to provide the physical plasma parameter (e.g., collision frequencies, cyclotron frequency, densities, and conductivities) and the geomagnetic field at the E region height to allow the computations of the zonal component of the electric field, a magnetic field-aligned-integrated conductivity model was developed for proving the conductivities using the IRI-2007, the MSIS-2000, and the IGRF-11 models as input parameters for ionosphere, neutral atmosphere, and Earth magnetic field, respectively. This model was originally developed by *Denardini* [2007], and several other updates have being applied since then, like the ion-neutron collision frequencies of all the species to be combined through the momentum transfer collision frequency equation.

Table 1. Error Estimating the E_y and E_z With Artificial 10% Error Simultaneously Introduced to the Outputs From the MSIS-2000, IGRF-11, and IRI-2007 Models for Four Range Heights

Altitude (km)	δE_y (%)		δE_z (%)	
	Models - 10%	Models + 10%	Models - 10%	Models + 10%
110.3	-04.79	+05.37	-11.10	+11.48
107.7	-08.71	+09.99	-13.01	+14.05
105.1	-15.72	+18.80	-17.06	+19.49
102.5	-22.00	+27.30	-20.38	+23.96
Error	12.81	15.37	15.39	17.25

Due to the quantity of variables involved in such computations, we have investigated the magnitude of the error for computing the E_y that may arise from eventual errors coming from the model inputs. The analysis constituted of artificially increasing/decreasing the magnitude of the model outputs by 10% and evaluating the impact on the E_y . The effects were investigated considering the artificially increasing/decreasing the magnitude of each model outputs separately and cumulatively. The variations were referred to the reference value of the electric field obtained without any change in quantities provided by the models. This study may offer substantial discussion in itself, and therefore, its results are not presented or discussed here. We would only mentioned that the main results obtained from the analysis of the MSIS-2000 model can be responsible for the highest percentage of uncertainty when deriving the electric fields, followed by IGRF-11 and IRI-2007 models. However, we present some finding from the above analysis concerning the present work, considering that all models are introducing an error of 10% in a cumulative way only. Table 1 summarizes the results of our findings for the E_y and E_z , at the four different radar range heights where we calculated the electric field.

From this analysis, we observe that E_y may have an error of 27.30% in relation to the reference date and the E_z component of 23.96%, both in the lower region of EEJ. It should be noted that all these errors are much smaller (at least twice) than the uncertainty associated with the Doppler velocity measurements from the RESCO radar mentioned in the previous section (2.42% in average). Also, smaller errors are concentrated in the upper portion of the EEJ. In terms of cause-effect relationship, a 10% reduction (increase) in quantities provided by the models reduces (increases) both E_y and E_z in all range heights. These features are easily identified in the graphs in Figure 1. The black curves (dots) represent the reference E_y (left) and E_z (right) profiles obtained without any change in quantities provided by the models. The dashed curves (triangles) represent the same profiles obtained with reducing the quantities provided by the models, while the dash-dotted curves (squares) represent the same profiles obtained with increasing these quantities. The error bars provide the experimental variations of the component between 8 h and 18 h (LT).

The influence of empirical models IRI-2007, MSIS-2000, and IGRF-11 is therefore a concern that must be taken into consideration while evaluating our results. Indeed, *Alken and Maus [2010]* performed similar model

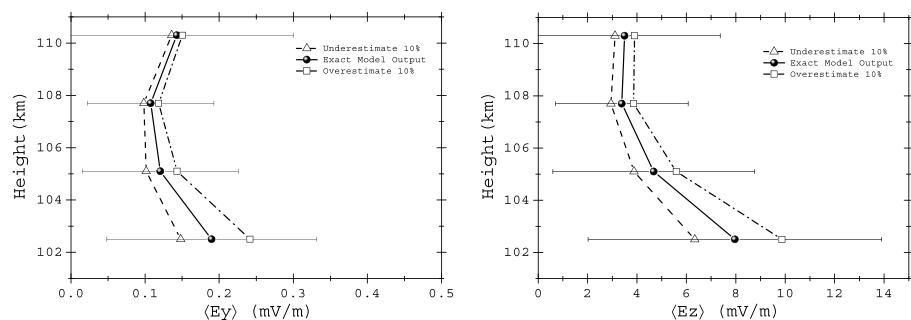


Figure 1. Vertical profile of the E_y and E_z using the model output (dots), including the error bars associated with measurements, same profiles with artificial reduction of 10% (triangles) in the models (MSIS-2000, IGRF-11, and IRI-2007) outputs, and same profiles with artificial addition of 10% (squares) to the models outputs.

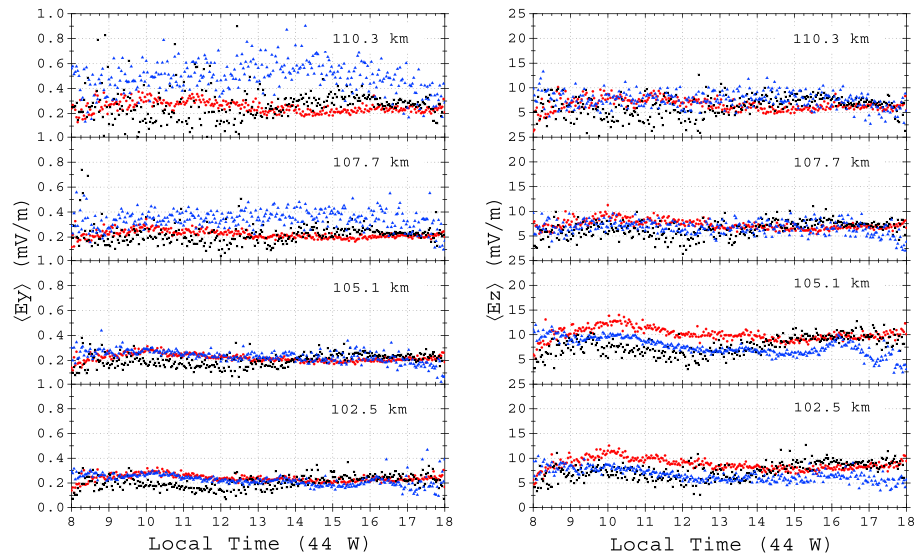


Figure 2. Diurnal variation of the E_y and E_z for high (red dots), average (black squares), and low (blue triangles) solar activities.

impact studies when deriving E_y from the CHAMP satellite using IRI-2007 and the MSIS-2000 for obtaining the conductivities. They investigated the impact on E_y of increasing and decreasing the electron temperature, electron density, collision frequencies, and neutral densities in the models and found IRI-2007 model to be the main source of uncertainty. *Bilitza and Reinisch [2008]*, *Picone et al. [2002]*, and *Finlay et al. [2010]* did not describe or comment about any potential errors associated with IRI-2007, MSIS-2000, and IGRF-11 models although.

In summary, despite we have made an extensive search in the published uncertainties related to the models used in this study, we were only able to find the study published by *Abdu et al. [2004]*, which pointed out that the IRI model underestimates the E region peak density in the Brazilian sector (see, for example, Figure 4 in their work). However, once we have no knowledge of other empirical models available for the Brazilian sector, we assume that their results are the best information available, but the discussion provided in this section shall be kept in mind when evaluating our results.

3. Results and Discussion

The mean diurnal variation of the E_y and E_z (geomagnetic quiet days only) with no interference in quantities provided by the input models was then classified according to the $F_{10.7}$. They are considered to be acquired during high solar activity when the radar soundings were performed at $F_{10.7}$ greater than or equal to 150. These electric fields are considered to be computed for average solar activity when the radar soundings were performed at $F_{10.7}$ between 100 and 150. Finally, the obtained values are considered to be computed for low solar activity, when the radar soundings were carried out at $F_{10.7}$ less than or equal to 100. After the classification, we performed the sample mean and standard deviations for all the E_y and E_z (per range height) available for the Brazilian sector over this period of study.

The results of the diurnal variations of the E_y and E_z per range height are shown in Figure 2, for the three solar flux conditions considered in the present analysis. The red dots represent the diurnal variations of the E_y (left) and E_z (right) obtained for the high solar activity for the four range heights of the radar soundings. The black squares represent the same diurnal variation obtained for average solar activity, while the blue triangles represent the diurnal variability during low solar activity.

Considering E_y only, we are not able to clearly identify the influence of the solar activity in its diurnal variation, independent of the height, except at 110.3 km at high solar activity when we have considerable data dispersions. These graphs showed that E_y ranges from 0.19 to 0.35 mV/m between the 8 and 18 h (LT) in the Brazilian sector and seems to have a small dependency with the solar activity. In regard to the E_z , it

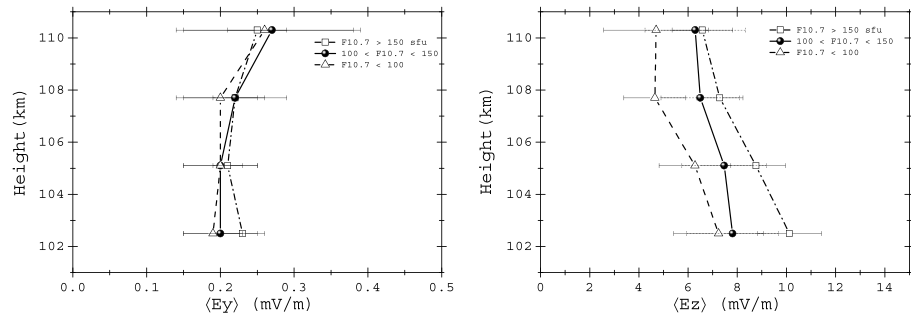


Figure 3. Vertical profiles of the (left) E_y and (right) E_z estimate during low (triangles with dashed lines), average (dots with solid line), and high (squares with dash-dotted lines) solar activity level based on the $F_{10.7}$ solar flux.

is notable that it is more intense during high solar flux, especially in the morning hours from 9 and 13 h (LT) over all range heights. The E_z ranges from 4.65 to 10.12 mV/m and offers a more pronounced dependency as observed.

In order to investigate further the height dependence of the electric field with solar activity, we calculated the daily average E_y and daily average E_z , and their standard deviations. These average values presented in the vertical profiles shown in Figure 3, and the precise values are listed in Table 2.

Analyzing these average results, we observe a positive gradient of E_y with height for low and average solar activity. During high solar activity we identify higher values of E_y at lower altitudes (102 km). Also, the higher E_y (0.27 mV/m) is found during average solar activity in the upper range height (110 km), while the lower E_y (0.19 mV/m) is found low average solar activity in the lower range height (102 km). With regard to the gradient of E_z , we identified a negative gradient irrespective of the solar activity. However, there is a directly proportional dependence of the E_z with the solar activity, i.e., the higher the solar activity, the higher the E_z , in all the range heights. Further, we identify that as the $F_{10.7}$ increases, the E_y increases at the lower portion of EEJ (below 105–107 km) and decreases in the upper portion (above 107 km).

At this point, it is important to stress that $F_{10.7}$ does not actually interact with the Earth’s atmosphere. However, $F_{10.7}$ is considered to be a good generalized solar proxy for EUV irradiances which ionizes it. Bruevich *et al.* [2014] stated that it is originated in the cool corona, a solar region that is closely coupled with magnetic structures responsible for creating the XUV-EUV irradiances. Also, $F_{10.7}$ depends on few processes. Therefore, it is reasonable to assume that EUV solar flux varies with $F_{10.7}$ [Chatterjee and Das, 1995]. The EUV spectra from 800 and 1027 Å absorbed by the molecular oxygen to form O_2^+ , while the EUV with wavelength between 1027 and 1118 Å is responsible for the ionization of the minor constituents as well as for driving the molecular oxygen to the excited state $O_2(^1\Delta_g)$. Therefore, there is greater availability of ionizing radiation to the extent that the $F_{10.7}$ solar flux increases, and the more the ionizing radiation, the greater the electron density.

Table 2. Daily Average of E_y (mV/m) and E_z (mV/m) Per Radar Range Height and Solar Activity Level, Including the Corresponding Standard Deviation

$F_{10.7}$ Solar Flux (sfu)	Height (km)	$\langle E_y \rangle \pm \langle SD \rangle$	$\langle E_z \rangle \pm \langle SD \rangle$
High ($F_{10.7} \geq 150$)	110.3	0.25 ± 0.04	6.58 ± 1.23
	107.7	0.22 ± 0.03	7.29 ± 0.94
	105.1	0.21 ± 0.02	8.76 ± 1.20
	102.5	0.23 ± 0.03	10.12 ± 1.30
Average ($100 < F_{10.7} < 150$)	110.3	0.27 ± 0.12	6.29 ± 2.04
	107.7	0.22 ± 0.07	6.50 ± 1.60
	105.1	0.20 ± 0.05	7.47 ± 1.72
	102.5	0.20 ± 0.05	7.81 ± 1.87
Low ($F_{10.7} \leq 100$)	110.3	0.26 ± 0.12	4.70 ± 2.13
	107.7	0.20 ± 0.06	4.65 ± 1.26
	105.1	0.20 ± 0.05	6.28 ± 1.46
	102.5	0.19 ± 0.04	7.24 ± 1.82

From our analysis on the models effecting the electric field computation, we identified that adding up 10% of electron density in the IRI-2007 will lead to an increase of 2.86% in E_y at 102.5 km height and reduces it in the upper range heights (not shown here). Accordingly, the increase in the solar flux $F_{10.7}$ causes an increase ionization which leads to an increase of electron density that causes an increase in E_y lower portion of EEJ and reduces E_y at the top, which explains the results in Figure 2 and Table 2.

Finally, despite studies from Fejer [1991], Fejer et al. [1991], and Santos et al. [2013] that show evidence that $F_{10.7}$ flux represented solar activity affecting the vertical plasma drift at the F region during the prereversal peak, we could not identify significant differences in the amplitude of the electrical field at the E region range heights investigated, since the values lied on the average deviations range, which represent the diurnal variability of the electric field components.

4. Summary and Conclusions

We were able to clearly identify an E_z dependence on solar activity but could not find any for E_y . E_z is notably more intense during periods of high solar flux over all altitude ranges, especially during morning hours between 9 and 13 h (LT).

We observe a positive gradient of E_y with height for low and average solar activity analyzing the daily average E_y , but not during high solar activity. The gradient of E_z remained negative irrespective of solar activity, and a proportional dependence of E_z with solar activity is clearly observed, in all the range heights.

We also identify that the E_y increases at the lower portion of EEJ (below 105–107 km) and decreases in the upper portion (above 107 km) as the $F_{10.7}$ flux increases. A tentative explanation was presented in terms of the increase in the $F_{10.7}$ solar flux causing an increase in ionization that then leads to an increase in electron density. This causes an increase in E_y in the lower portion of the EEJ and reduces E_y at the top of the EEJ. This is found through our IRI-2007 analysis of the electric field computation.

In conclusion, the zonal electric field, which normally ranged from 0.19 to 0.35 mV/m between 8 and 18 h (LT) in the Brazilian sector, presented a small dependency with the solar activity. The vertical electric field, which normally ranges from 4.65 to 10.12 mV/m, presented a more pronounced dependency although. But we see no appreciable dependence in the amplitude of the electrical field at the E region range heights investigated since the values lied on the average deviations range.

Acknowledgments

C.M. Denardini thanks CNPq/MCTI (grant 303121/2014-9), FAPESP (grant 2012/08445-9), and to the Brazilian Government (program 2056, Budget Action N387, and Budget Plan 08/2013-2017), which supported both the scientific and infrastructure projects that gave birth to the Embrace/INPE Program. J. Moro thanks to CNPq/MCTI (grant 300702/2015-9). L.C.A. Resende thanks to FAPESP (grant 2014/11198-9). S.S. Chen thanks to CNPq/MCTI (grant 303806/2013-3). C. M. Denardini (corresponding author) is currently the responsible for the RESCO Radar and its operation, and the data used for developing the present work stays under his safeguard. Any data request shall then be sent to him through the provided e-mail address.

Alan Rodger thanks two reviewers for their assistance in evaluating this paper.

References

- Abdu, M. A., I. S. Batista, B. W. Reinisch, and A. J. Carrasco (2004), Equatorial Flayer heights, evening prereversal electric field, and night E -layer density in the American sector: IRI validation with observations, *Adv. Space Res.*, 34(9), 1953–1965.
- Alken, P., and S. Maus (2010), Electric fields in the equatorial ionosphere derived from CHAMP satellite magnetic field measurements, *J. Atmos. Sol. Terr. Phys.*, 72(4), 319–326.
- Aveiro, H. C., C. M. Denardini, and M. A. Abdu (2009a), Climatology of gravity waves–induced electric fields in the equatorial E region, *J. Geophys. Res.*, 114, A11308, doi:10.1029/2009JA014177.
- Aveiro, H. C., C. M. Denardini, and M. A. Abdu (2009b), Signatures of 2-day wave in the E -region electric fields and their relationship to winds and ionospheric currents, *Ann. Geophys.*, 27(2), 631–638.
- Balsley, B. B. (1969), Some characteristics of non-two-stream irregularities in equatorial electrojet, *J. Geophys. Res.*, 74(A9), 2333–2347, doi:10.1029/JA074i009p02333.
- Bard, Y. (1974), *Nonlinear Parameter Estimation*, pp. 146–151, Academic Press, New York.
- Billitza, D., and B. Reinisch (2008), International Reference Ionosphere 2007: Improvements and new parameters, *Adv. Space Res.*, 42(4), 599–609.
- Bruevich, E. A., V. V. Bruevich, and G. V. Yakunina (2014), Changed relation between solar 10.7-cm radio flux and some activity indices which describe the radiation at different altitudes of atmosphere during cycles 21–23, *J. Astrophys. Astron.*, 35, 1–15.
- Campbell, W. H. (1989), An introduction to quiet daily geomagnetic fields, *Pure Appl. Geophys.*, 131(3), 315–331.
- Chatterjee, T. N., and T. K. Das (1995), Relation between solar UV flux and 10.7-cm radio-emission, *Mon. Not. R. Astron. Soc.*, 274(3), 858–860.
- Cohen, R. (1973), Phase velocities of irregularities in equatorial electrojet, *J. Geophys. Res.*, 78(A13), 2222–2231, doi:10.1029/JA078i013p02222.
- Cohen, R., and K. L. Bowles (1967), Secondary irregularities in equatorial electrojet, *J. Geophys. Res.*, 72(A3), 885–894, doi:10.1029/JZ072i003p00885.
- Denardini, C. M. (2007), A conductivity model for the Brazilian equatorial E -region: Initial results, *Braz. J. Geophys.*, 25(2), 87–94.
- Denardini, C. M., M. A. Abdu, and J. H. A. Sobral (2003), Detection of three distinct regions in the equatorial electrojet in the Brazilian sector, *Braz. J. Geophys.*, 21(1), 65–74.
- Denardini, C. M., M. A. Abdu, and J. H. A. Sobral (2004), VHF radar studies of the equatorial electrojet 3-m irregularities over Sao Luis: Day-to-day variabilities under auroral activity and quiet conditions, *J. Atmos. Sol. Terr. Phys.*, 66(17), 1603–1613.
- Denardini, C. M., M. A. Abdu, E. R. de Paula, J. H. A. Sobral, and C. M. Wrasse (2005), Seasonal characterization of the equatorial electrojet height rise over Brazil as observed by the RESCO 50 MHz back-scatter radar, *J. Atmos. Sol. Terr. Phys.*, 67(17–18), 1665–1673.

- Denardini, C. M., M. A. Abdu, E. R. de Paula, C. M. Wrasse, and J. H. A. Sobral (2006), VHF radar observations of the dip equatorial *E*-region during sunset in the Brazilian sector, *Ann. Geophys. Hydrospheres Space Sci.*, *24*(6), 1617–1623.
- Denardini, C. M., M. A. Abdu, H. C. Aveiro, L. C. A. Resende, P. D. S. C. Almeida, E. P. A. Olivio, J. H. A. Sobral, and C. M. Wrasse (2009), Counter electrojet features in the Brazilian sector: Simultaneous observation by radar, digital sounder and magnetometers, *Ann. Geophys.*, *27*(4), 1593–1603.
- Denardini, C. M., H. C. Aveiro, P. D. S. C. Almeida, L. C. A. Resende, L. M. Guizelli, J. Moro, J. H. A. Sobral, and M. A. Abdu (2011), Daytime efficiency and characteristic time scale of interplanetary electric fields penetration to equatorial latitude ionosphere, *J. Atmos. Sol. Terr. Phys.*, *73*(11–12), 1555–1559.
- Denardini, C. M., H. C. Aveiro, J. H. A. Sobral, J. V. Bageston, L. M. Guizelli, L. C. A. Resende, and J. Moro (2013), *E* region electric fields at the dip equator and anomalous conductivity effects, *Adv. Space Res.*, *51*(10), 1857–1869, doi:10.1016/j.asr.2012.06.003.
- Farley, D. T. (1963), A plasma instability resulting in field aligned irregularities in the ionosphere, *J. Geophys. Res.*, *68*(A22), 6083–6097, doi:10.1029/JZ068i022p06083.
- Farley, D. T. (1985), Theory of equatorial electrojet plasma waves: New developments and current status, *J. Atmos. Terr. Phys.*, *47*(8–10), 729–744.
- Fejer, B. G. (1991), Low latitude electrodynamic plasma drifts: A review, *J. Atmos. Terr. Phys.*, *53*, 677–693.
- Fejer, B. G., and M. C. Kelley (1980), Ionospheric irregularities, *Rev. Geophys.*, *18*(2), 401–454, doi:10.1029/RG018i002p00401.
- Fejer, B. G., E. R. de Paula, S. A. Gonzalez, and R. F. Woodman (1991), Average vertical and zonal *F*-region plasma drifts over Jicamarca, *J. Geophys. Res.*, *96*(A8), 13,901–13,906, doi:10.1029/91JA01171.
- Finlay, C. C., et al. (2010), International geomagnetic reference field: The eleventh generation, *Geophys. J. Int.*, *183*, 1216–1230.
- Guizelli, L. M., C. M. Denardini, J. Moro, and L. C. A. Resende (2013), Climatological study of the daytime occurrence of the 3-meter EEJ plasma irregularities over Jicamarca close to the solar minimum (2007 and 2008), *Earth Planets Space*, *65*(1), 39–44.
- Hanuise, C., and M. Crochet (1978), Oblique HF radar studies of plasma instabilities in equatorial electrojet in Africa, *J. Atmos. Terr. Phys.*, *40*(1), 49–59.
- Hysell, D. L., and J. D. Burcham (2000), Ionospheric electric field estimates from radar observations of the equatorial electrojet, *J. Geophys. Res.*, *105*(A2), 2443–2460, doi:10.1029/1999JA900461.
- Mayaud, P. N. (1977), Equatorial counter-electrojet—A review of its geomagnetic aspects, *J. Atmos. Terr. Phys.*, *39*(9–10), 1055–1070.
- Patra, A. K., D. Tiwari, C. V. Devasia, T. K. Pant, and R. Sridharan (2005), East-west asymmetries of the equatorial electrojet 8.3 m type-2 echoes observed over Trivandrum and a possible explanation, *J. Geophys. Res.*, *110*, A11305, doi:10.1029/2005JA011124.
- Picone, J. M., A. E. Hedin, D. P. Drob, and A. C. Aikin (2002), NRLMSISE-00 empirical model of the atmosphere: Statistical comparisons and scientific issues, *J. Geophys. Res.*, *107*(A12), 1468, doi:10.1029/2002JA009430.
- Prakash, S., S. P. Gupta, B. H. Subbaray, and C. L. Jain (1971), Electrostatic plasma instabilities in equatorial electrojet, *Nat. Phys. Sci.*, *233*(38), 56–58.
- Press, W. H., S. A. Teukolsky, W. T. Vetterling, and B. P. Flannery (1992), *Numerical Recipes in C: The Art of Scientific Computing*, 994 pp., Cambridge Univ. Press, Cambridge, U. K.
- Reddy, C. A., and C. V. Devasia (1976), Short-period fluctuations of equatorial electrojet, *Nature*, *261*(5559), 396–397.
- Reddy, C. A., and C. V. Devasia (1981), Height and latitude structure of electric-fields and currents due to local east-west winds in the equatorial electrojet, *J. Geophys. Res.*, *86*(A7), 5751–5767, doi:10.1029/JA086iA07p05751.
- Resende, L. C. A., and C. M. Denardini (2012), Equatorial sporadic *E*-layer abnormal density enhancement during the recovery phase of the December 2006 magnetic storm: A case study, *Earth Planets Space*, *64*(4), 345–351.
- Resende, L. C. A., C. M. Denardini, and I. S. Batista (2013), Abnormal fbEs enhancements in equatorial *Es* layers during magnetic storms of solar cycle 23, *J. Atmos. Sol. Terr. Phys.*, *102*, 228–234.
- Santos, A. M., M. A. Abdu, J. H. A. Sobral, M. Mascarenhas, and P. A. B. Nogueira (2013), Equatorial evening prereversal vertical drift dependence on solar EUV flux and $F_{10.7}$ index during quiet and disturbed periods over Brazil, *J. Geophys. Res. Space Physics*, *118*, 4662–4671, doi:10.1002/jgra.50438.
- Shume, E. B., C. M. Denardini, E. R. de Paula, and N. B. Trivedi (2010), Variabilities of the equatorial electrojet in Brazil and Peru, *J. Geophys. Res.*, *115*, A06306, doi:10.1029/2009JA014984.
- Shume, E. B., E. R. de Paula, E. A. Kherani, M. A. Abdu, and C. M. Denardini (2011), Equatorial electrojet plasma irregularities observed during late afternoon by the 30 MHz coherent scatter radar in Sao Luis, Brazil, *J. Atmos. Sol. Terr. Phys.*, *73*(11–12), 1560–1567.
- Sugiura, M., and J. C. Cain (1966), A model equatorial electrojet, *J. Geophys. Res.*, *71*(A7), 1869–1877, doi:10.1029/JZ071i007p01869.